Progress In Electromagnetics Research C, Vol. 125, 147–159, 2022

A Diesel-Electric Hybrid Field Modulation Motor with Bread-Loaf Eccentric Magnetic Pole for Ship Propulsion

Weizhao Tang, Libing Jing*, and Lianhua Zheng

Abstract—In order to improve the reliability and continuous navigation of ship propulsion, a diesel-electric hybrid field modulation motor with bread-loaf eccentric magnetic poles is proposed in this paper. The permanent magnet of the inner rotor of the motor adopts a bread-loaf eccentric magnetic pole structure and is embedded and fixed on the iron yoke of the inner rotor. The structure can obtain a sinusoidal air gap magnetic field, to reduce the torque ripple of the motor. In this study, some key parameters of the motor are optimized by using the optimization strategy of the combination of genetic algorithm and finite element method. In addition, compared with the conventional magnetic field modulation motor with surface mounted permanent magnet, the motor has a stronger rotor structure. The back-EMF, torque, and loss of the motor are calculated. The proposed motor has good sinusoidal back-EMF, less loss and better stability. Finally, the working modes of the motor in the diesel-electric hybrid ship propulsion system are mainly diesel internal combustion engine driving mode, electric propulsion mode, and hybrid propulsion mode. The system can improve the reliability and continuous navigation of the ship propulsion system.

1. INTRODUCTION

With the continuous development of ship electric propulsion technology, it is a necessary trend under the severe situation of energy and environment [1, 2]. Compared with fuel-driven ships, diesel-electric hybrid ships have the advantages of high fuel efficiency and good maneuverability and have better flexibility in power distribution between propulsion and load [3]. Ship propulsion system is generally used to drive low-speed and high torque loads [4]. At present, a ship propulsion system mainly adopts a permanent magnet synchronous motor or permanent magnet brushless DC motor combined with mechanical gear to realize low-speed and high torque transmission [5]. However, gears produce mechanical vibration and noise. In addition, in the case of overload, the friction loss and even damage to mechanical gears may be increased. The introduction of coaxial magnetic gear (CMG) can overcome the above problems, because the CMG has the advantages of overload protection, no lubrication, and low noise [6, 7], so as to prolong the service life of the propulsion system.

Diesel-electric hybrid field modulation motor with bread-loaf eccentric magnetic poled belongs to magnetic field modulation motor, which works based on the principle of magnetic field modulation. In [8], the authors proposed a magnetic gear motor integrated with coaxial magnetic gear and synchronous motor, which can effectively improve the output torque. In [9], the authors adopted the integrated magnetic field modulation brushless double rotor motor with an improved permanent magnet (PM) rotor, which can realize magnetic speed change and low and high torque outputs. Magnetic field-modulated brushless dual rotor motor can also realize low-speed and high torque operation, and is also applied in hybrid power [10]. To further reduce the torque ripple of the motor, the key parameters of the motor model are optimized. There are many motor optimization methods, such as Taguchi method,

Received 16 June 2022, Accepted 3 October 2022, Scheduled 15 October 2022
* Corresponding author: Libing Jing (jinglibing163@163.com).
The authors are with the College of Electrical Engineering & New Energy, China Three Gorges University, Yichang 443002, China.

Response surface method (RSM), and genetic algorithm (GA) [11–13]. Algorithm optimization based on finite element method (FEM), such as genetic algorithm, has very high accuracy to obtain the optimal solution. Therefore, genetic algorithm is very suitable for motor parameter optimization.

In this paper, the inner rotor permanent magnet of the proposed motor adopts a bread-loaf eccentric magnetic pole and is embedded and fixed on the iron yoke of the inner rotor. The armature magnetic field and the inner and outer rotor permanent magnetic fields are modulated by magnetic adjusting teeth and coupled with each other to achieve low-speed and high torque output. The main advantages of the proposed motor are that the number of mechanical gear devices and stator slots of the motor in the marine propulsion system is reduced with small size of the proposed motor; the output torque is large; the loss of the motor is reduced; and the efficiency of the motor is improved. Among them, as the power source of diesel-electric hybrid ship propulsion motors, there are diesel internal combustion engines and electric propulsion. In Section 2, the system introduces the topology and working principle of the motor. In Section 3, the genetic algorithm and finite element method are combined to optimize the motor model. In Section 4, the electromagnetic performance of the motor is calculated. Finally, some conclusions are drawn in Section 5.

2. TOPOLOGY AND OPERATION PRINCIPLE

Figure 1(a) and Figure 1(b) show the topology of the proposed motor model and the conventional motor model, respectively. The two motors have two layers of air gap, including stator, magnetic adjusting teeth, outer rotor, and inner rotor.

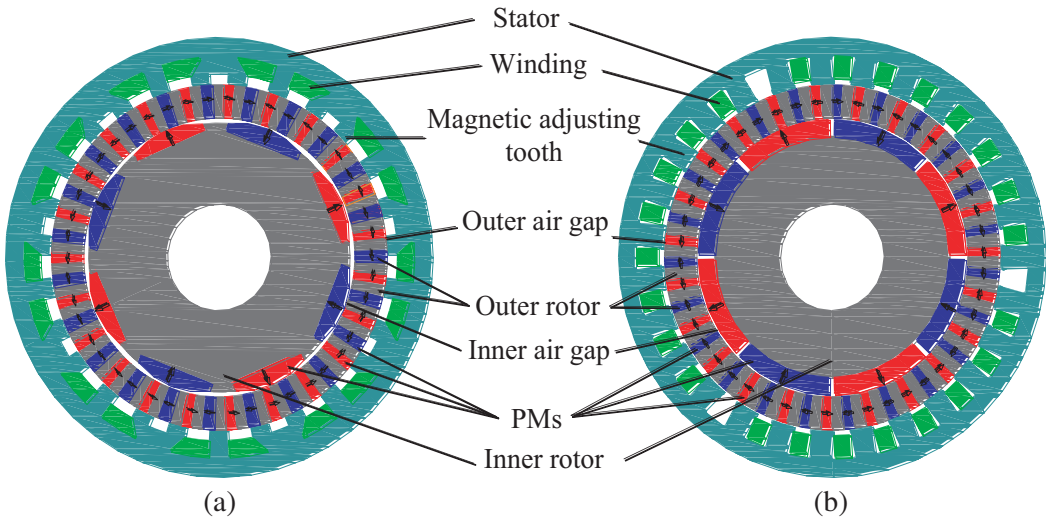

Figure 1. The topology of motor. (a) Proposed model; (b) Conventional model.

Figure 2 shows that the inner rotor permanent magnet of the proposed motor model is a bread-loaf eccentric magnetic pole structure. The permanent magnet of the inner rotor is embedded and fixed on the iron yoke of the inner rotor, which is conducive to the stability of the rotor structure. In addition, the inner air gap of the proposed motor model is a nonuniform air gap, in which a sinusoidal air gap magnetic field can be obtained to reduce the torque ripple of the motor.

The working principle of the diesel-electric hybrid field modulation motor with bread-loaf eccentric magnetic poles for ship propulsion can be divided into a coaxial magnetic gear, a permanent magnet brushless motor, and a vernier permanent magnet motor. The torque of the inner rotor is also composed of two parts, namely, the electromagnetic torque T_{ein} and diesel-engine torque T_d. Then, the resultant torque on the inner rotor T_{in} and the torque on the outer rotor T_{out} follow the torque ratio of the CMG. Therefore, their torque relationship can be expressed as:

$$\begin{cases} T_{in} = T_d \pm T_{ein} \\ T_{out} = G_r \cdot T_{in} \end{cases} \tag{1}$$

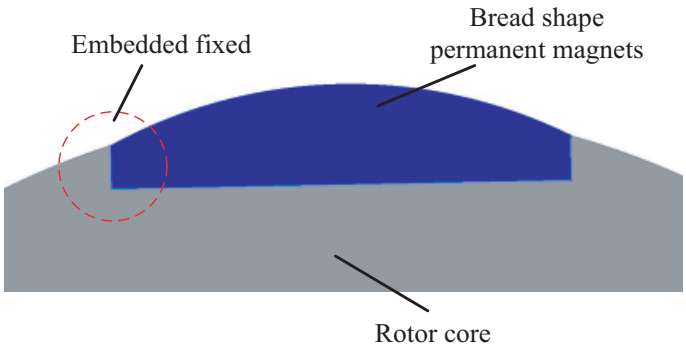

Figure 2. Structure of bread-loaf eccentric magnetic pole of inner rotor permanent magnet.

where the symbol "±" indicates that the electromagnetic torque from the PMSM part can be in the same and opposite directions as the torque of the diesel-engine. If the direction is the same, the PMSM part works as a motor; otherwise, it will work as a generator.

The number of magnetic adjusting teeth is N_t; the pole pairs of the permanent magnet of the outer rotor is P_o; and the pole pairs of the permanent magnet of the inner rotor are P_i. The formula is as follows:

$$N_t = P_o + P_i \tag{2}$$

According to the principle of magnetic field modulation, the working principle of the proposed motor model is similar to that of coaxial magnetic gear [14]. Therefore, the spatial harmonic pole pairs contained in the air gap magnetic field are expressed as:

$$P_{m,k} = |mP + kN_t| \tag{3}$$

where $k = 0, \pm1, \pm2, \ldots, \infty$; $m = 1, 3, \ldots, \infty$; P is the number of poles generated by the inner and outer rotors, and N_t is the number of magnetic adjusting teeth.

The harmonic component in the air gap has a specific space polar number and speed. As can be seen from [15], the angular velocity of the space harmonic component in the inner and outer air gap is expressed as:

$$\Omega_{m,k} = \frac{mP}{mP + kN_t}\Omega_r + \frac{kN_t}{mP + kN_t}\Omega_t \tag{4}$$

where Ω_m is the angular velocity of spatial harmonic component; Ω_r is the angular velocity of rotor; and Ω_t is the angular velocity of magnetic adjusting teeth.

When $m = 1$ and $k = -1$, the air gap magnetic field modulated by the magnetic adjusting teeth is the strongest. The inner rotor and outer rotor rotate in a constant proportion. The speed is as follows:

$$G_r = \frac{P_i - N_t}{P_i} \tag{5}$$

According to the proposed motor model parameters, the permanent magnet of the inner rotor generates 4 pairs of pole magnetic field ($P_i = 4$); the total number of magnetic adjusting teeth is 27 ($N_t = 27$); the permanent magnet of the outer rotor has 23 pairs of poles ($P_o = 23$); and the speed regulation ratio is -5.75. A negative sign indicates that the rotation directions of the inner rotor and outer rotor are opposite.

Figure 3 shows the propulsion motor system of hybrid ship. The system has diesel engine driving mode, electric propulsion mode, and hybrid propulsion mode. The outer rotor, inner rotor, and magnetic adjusting teeth can work like CMG. This working mode is in diesel internal combustion engine driving mode in the propulsion system, which can reduce the gear device compared with the conventional permanent magnet motor propulsion system. The inner rotor is connected to the internal combustion engine while the output rotor is connected to the propeller. At the same time, the working mode can charge the electric propulsion device of the propulsion system, so as to improve the continuous navigation of ship propulsion.

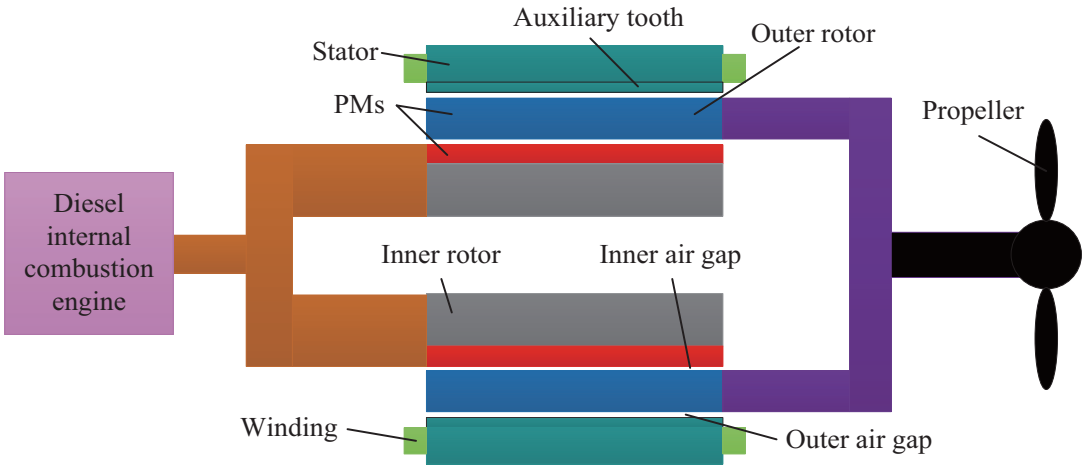

Figure 3. Diesel electric hybrid ship propulsion system.

3. MOTOR ANALYSIS AND OPTIMIZATION

Figure 4 shows some parameters of the stator structure. The genetic algorithm in ANSYS Maxwell is used to optimize the key parameters of the proposed motor. To make the stator core of the proposed motor model have better magnetic regulation function, it is necessary to optimize the thickness of the magnetic regulation teeth a, the thickness of the stator yoke b, and the radian of the magnetic regulation teeth d. These three parameters directly affect the air gap permeability distribution, and then affect the back-EMF waveform and torque ripple of the motor.

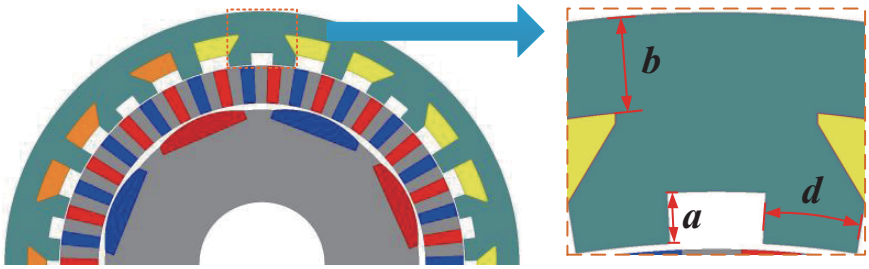

Figure 4. Some optimization parameters of stator structure.

The genetic algorithm is a random search algorithm based on the natural selection and natural genetic mechanism of biology. The basic idea of genetic algorithm is to use population search technology to represent the solution space with population and generate new population through genetic operations such as population selection, crossover, and mutation. This process continues until the population produces the optimal solution [16]. The genetic operation depends on genetic operators such as crossover operator ruler and mutation operator [17]. Figure 5 is the flowchart of motor genetic algorithm optimization.

The variation range of structural parameters of stator is:

$$\begin{cases} 3.5\,\text{mm} \le a \le 5.5\,\text{mm} \\ 6.5\,\text{mm} \le b \le 9.5\,\text{mm} \\ 5\ \text{deg} \le d \le 7\ \text{deg} \end{cases} \tag{6}$$

The roulette model is characterized by the higher the individual fitness, the higher the probability

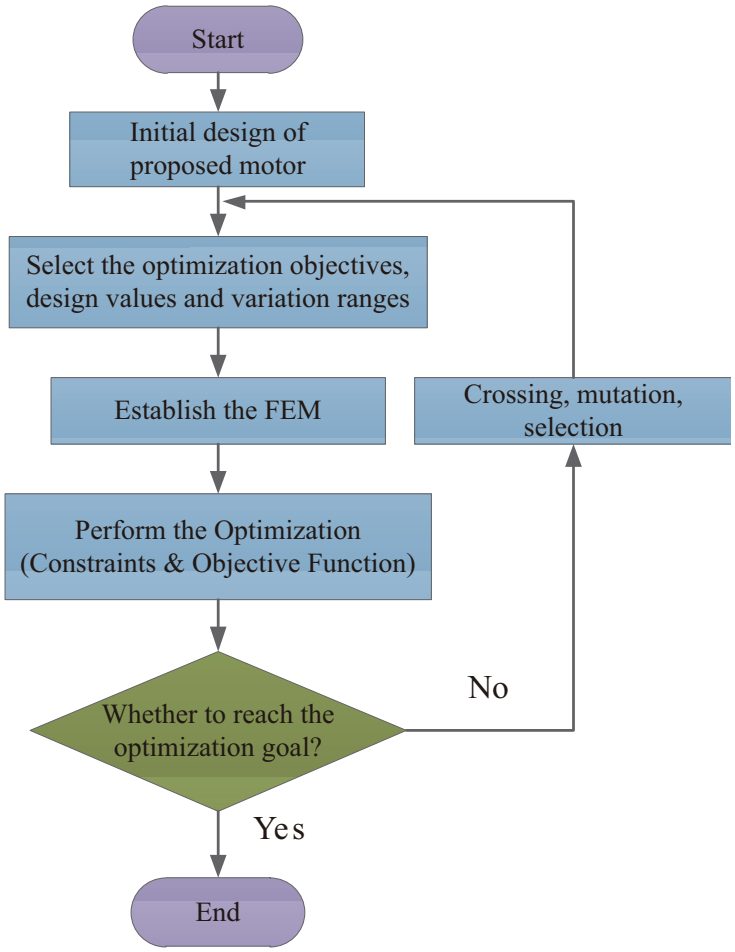

Figure 5. Flow chart of genetic algorithm optimization.

being drawn. This probability can be expressed as:

$$p_i = \frac{f(x_k)}{\sum_{j=1}^{n} f(x_j)} \tag{7}$$

where $f(x)$ is the fitness matrix of the individual.

Taking the torque ripple of the inner rotor of the motor as the optimization objective, the basic parameter settings of genetic algorithm are listed in Table 1. The smaller the objective function value is, the better the design scheme will be. As shown in Figure 6, the objective function value curve optimized by genetic algorithm is shown. The objective value reaches the minimum at generation 302, with a value of 0.0234. The parameters are optimized by genetic algorithm listed in Table 2.

4. COMPARISON OF ELECTROMAGNETIC PERFORMANCE

4.1. Flux Density and Harmonics Analysis

Figure 7 shows the magnetic field distribution of the motor calculated by the finite element method. It can be seen that most of the magnetic field lines of the motor pass through the inner and outer air gaps to form a series magnetic circuit, and the magnetic field coupling between the inner rotor and outer rotor is strong. Some key parameters of the motor are listed in Table 3.

Table 1. Parameters of initial design and optimal design.

Basic parameters	Settings
Selection operation	Roulette
Cross operation	Two-point crossover
Mutation operation	Uniform variation
Population size (n)	100
Number of generations ($g_{\max}$)	500
Crossover probability (p_c)	0.9
Mutation probability (p_m)	0.01

Table 2. Parameters of initial design and optimal design.

Parameters	Initial	Optimal
Thickness of magnetic adjusting teeth (a)	4 mm	4.74 mm
Thickness of stator yoke (b)	7 mm	8.87 mm
Radian of magnetic adjusting teeth (d)	5.5°	6.1°

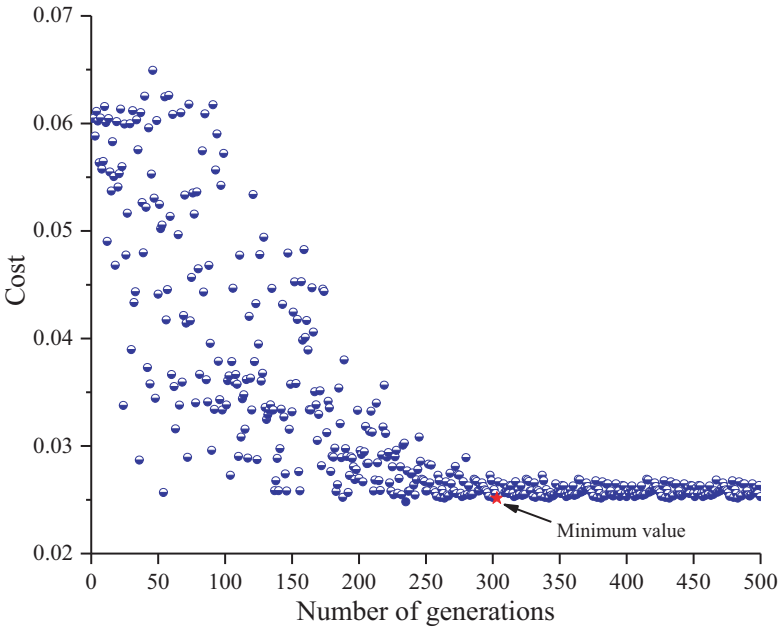

Figure 6. Optimization objective convergence diagram of genetic algorithm.

Figure 8 shows the radial flux density distribution in the outer air gap. It can be seen that the amplitude of the radial air gap flux density of the proposed motor model is slightly larger than that of the conventional radial air gap flux density. According to the principle of magnetic field modulation, the harmonic components with pole pairs equal to 4, 23, 31, 50, and 58 are working harmonics. Since the amount of inner rotor permanent magnet in the proposed model is less than that in the conventional model, the working harmonics of 23, 31, and 50 are smaller. The fourth harmonic component of the proposed model is larger than that of the conventional model, which can promote the torque transmission in the outer air gap.

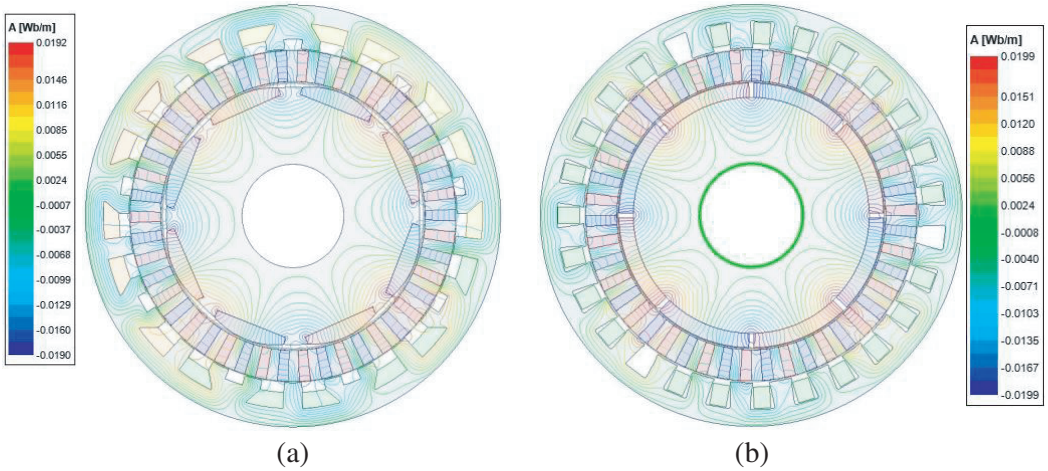

Figure 7. Flux line distributions under no-load condition. (a) Proposed model; (b) Conventional model.

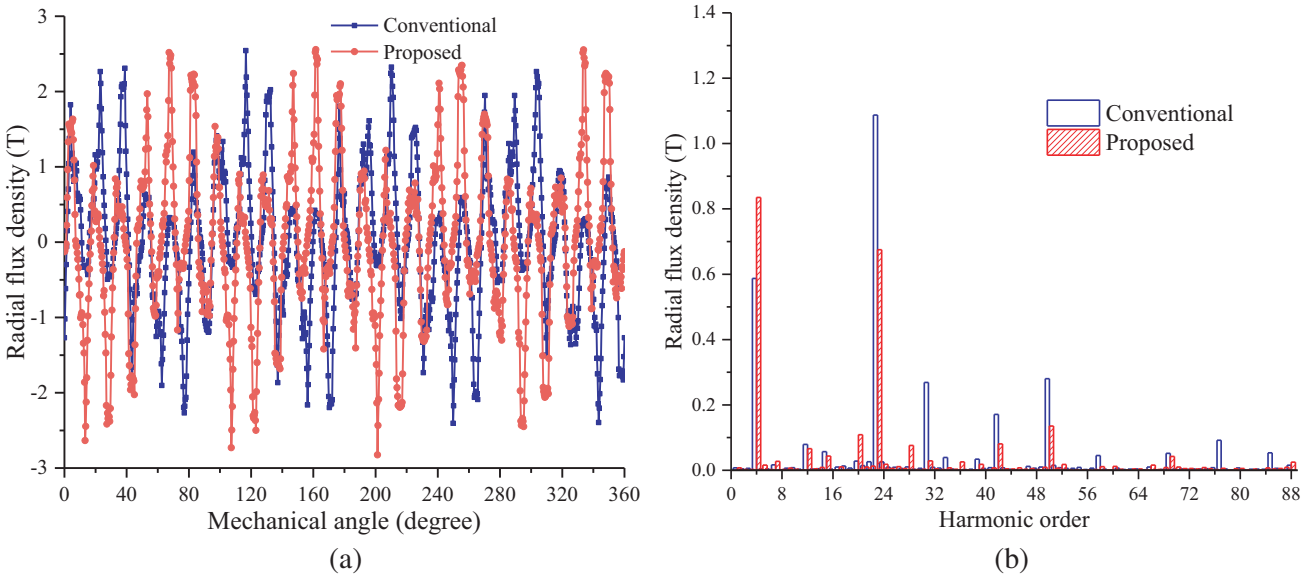

Figure 8. Radial flux density in the outer air gap. (a) Flux density distribution; (b) Harmonic spectra.

Table 3. Parameters of proposed motor model.

Parameter	Value
Outer radius of stator	102 mm
Inner radius of stator	81 mm
Outer radius of outer rotor	80 mm
Inner radius of outer rotor	65 mm
Outer radius of inner rotor	64 mm
Inner radius of inner rotor	25 mm
PMs material	NdFeB
Axial length	100 mm

Figure 9 shows the radial flux density waveform of the inner air gap. By changing the structure of the inner rotor permanent magnet, it can be seen from the figure that the radial air gap magnetic density waveform of the proposed model is closer to the sine wave. Compared with the conventional model, the 12th, 20th, 28th, and 36th nonworking harmonics of the proposed model are significantly suppressed, which helps to reduce the torque ripple of the motor and improve the stability of the motor.

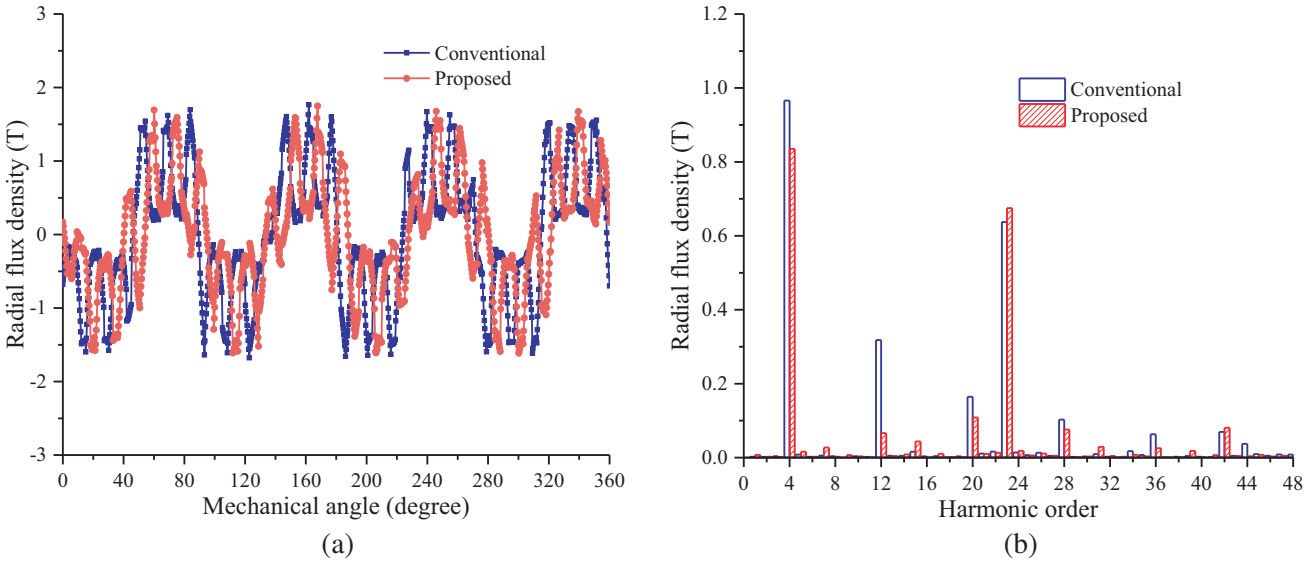

Figure 9. Radial flux density in the inner air gap. (a) Flux density distribution; (b) Harmonic spectra.

4.2. Back-EMF

During no-load operation of the motor, there is no current in the stator winding. The magnetic field on the rotor will generate rotating magnetic field in the air gap and cut the stator winding, so as to generate induced electromotive force in the stator winding, that is, no-load back-EMF, which can also be called no-load induced electromotive force. In this paper, the sinusoidal degree of no-load back-EMF waveform is measured by harmonic distortion rate. The smaller the total harmonic distortions (THD) rate of back-EMF is, the higher the sinusoidal degree of waveform is, which is expressed as:

$$THD = \frac{\sqrt{\sum_{i=2}^{n} B_{\delta i}^2}}{B_{\delta 1}} \times 100\% \tag{8}$$

where $B_{\delta 1}$ is the fundamental wave amplitude of the air gap magnetic flux density, $B_{\delta i}$ the amplitude of the first harmonic air gap magnetic flux density, and i the harmonic order.

Figure 10(a) shows the waveform of no-load back-EMF. It can be seen that the no-load back-EMF amplitudes of the proposed motor model and the conventional motor model are 59.75 V and 59.86 V, respectively. Figure 10(b) shows the harmonic spectrum of no-load back-EMF. After calculation, the harmonic distortion rate of the model is 6.384%, while that of the conventional model is 9.967%. Therefore, the sinusoidal degree of the no-load back-EMF waveform of this model is higher than that of the conventional model.

4.3. Torque

According to Maxwell stress tensor method [18], when the axial length is constant, the electromagnetic torque is directly proportional to the product of radial magnetic density and tangential magnetic density.

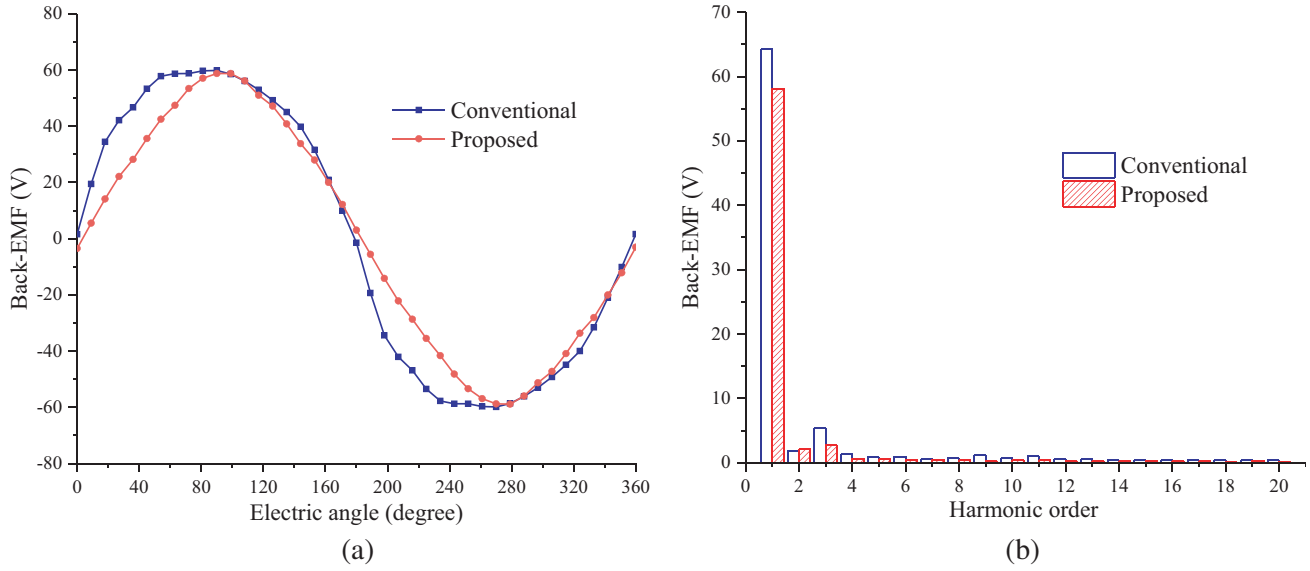

Figure 10. Back-EMF under no-load condition. (a) Waveform; (b) Harmonic spectra.

The torque expression is as follows:

$$T_{\text{em}} = \frac{L_{ef} R_e}{\mu_0} \int_0^{2\pi} B_r B_t d\theta \tag{9}$$

where L_{ef} is the effective axial length, R_e a circle of a radius in the air gap, μ the permeability of the vacuum, and B_r and B_t are the radial and tangential magnetic flux density, respectively.

The torque ripple coefficient b is introduced to represent the magnitude of torque ripple. The smaller the torque ripple coefficient is, the smaller the torque ripples is, the larger the torque ripple coefficient is, and the larger the torque ripples is. The b is defined as:

$$b = \frac{T_{\max} - T_{\min}}{T_{\text{avg}}} \tag{10}$$

where $T_{\max}$ is the maximum output torque, $T_{\min}$ the minimum output torque, and T_{avg} the average output torque.

When a symmetrical alternating current with an effective value of 5 A is connected to the armature winding, the electromagnetic torque waveforms of the inner rotor and the outer rotor are shown in Figure 11. It can be seen that the torque directions of the inner rotor and outer rotor are opposite. The average torques of the outer rotor and inner rotor of the proposed model are 109.65 N·m and 9.92 N·m higher than that of the conventional model, respectively. The average torque and torque ripple of the two motor models are calculated, as listed in Table 4.

Table 4. Torque and torque ripple.

	Type	$T_{\min}$ (N·m)	$T_{\max}$ (N·m)	T_{avg} (N·m)	b (%)
Inner rotor	Conventional	−35.06	−37.46	−36.32	6.61
	Proposed	−45.79	−46.87	−46.24	2.34
Outer rotor	Conventional	155.32	162.34	159.33	4.41
	Proposed	264.51	272.38	268.98	2.93

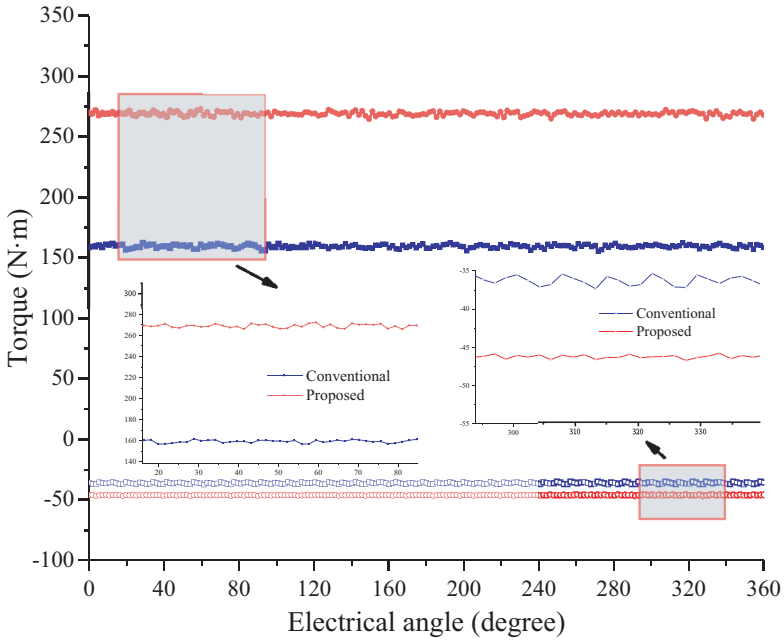

Figure 11. Electromagnetic torque.

4.4. Loss Analysis

The loss of diesel-electric hybrid ship propulsion motor mainly includes copper loss, core loss, and eddy current loss. The expression of copper loss is as follows:

$$P_{cu} = mI^2R \tag{11}$$

where m is the number of phases, I the phase current in the winding, and R the phase resistance of the stator winding.

This paper analyzes the core loss and eddy current loss of the proposed motor model, and studies the distribution law of core loss and eddy current loss. The core loss in permanent magnet motor mainly includes eddy current loss and hysteresis loss. The core loss is caused by the blocking effect of silicon steel material on the magnetic field, and the calculation formula of core loss P_c is:

$$P_c = K_h f B^2 + K_c f^2 B^2 + K_e f^{1.5} B^{1.5} \tag{12}$$

where K_h is the hysteresis loss coefficient, K_c the eddy current loss coefficient, K_e the additional loss coefficient, f the alternating frequency of magnetic field, and B the amplitude of magnetic flux density.

Due to the alternating magnetic field, the magnet produces eddy current loss. The simplified calculation formula of eddy current loss is:

$$P_e = \frac{Vb^2h^2}{2\rho\left(b^2+h^2\right)} \sum_{n=1} n^2 f_n^2 B_n^2 \tag{13}$$

where V is the volume of magnet, b the average width of permanent magnet, h the axial length of magnet, ρ the resistivity of permanent magnet, n the number of harmonics, f_n the relative motion frequency, B_n the amplitude of harmonic flux density.

Figure 12 shows the core loss cloud of the proposed motor model. It can be seen that since the magnetic adjusting teeth can change the air gap magnetic conductivity, there is a certain loss on the magnetic adjusting teeth, and the iron loss mainly occurs on the iron yoke of the inner rotor.

Figure 13, Figure 14, and Figure 15 show the copper loss waveform, core loss waveform, and eddy current loss waveform of the motor model, respectively. It can be seen from Figure 13 that the copper loss of the proposed model is 9.748 W, which is 5.495 W lower than that of the conventional model. According to Figure 14, the core loss of the proposed model and conventional model are 26.57 W

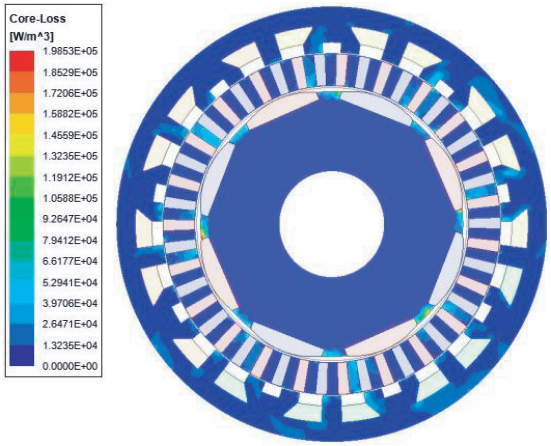

Figure 12. Core loss cloud of the proposed motor model.

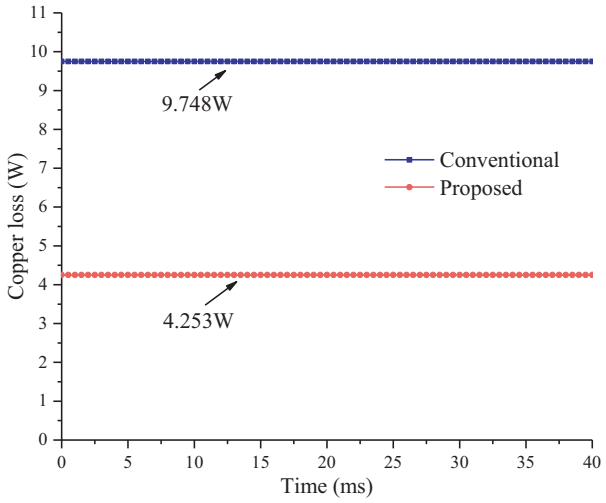

Figure 13. Copper loss.

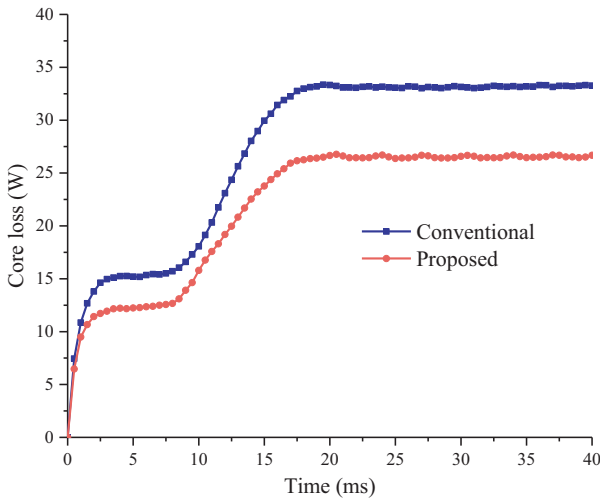

Figure 14. Core loss.

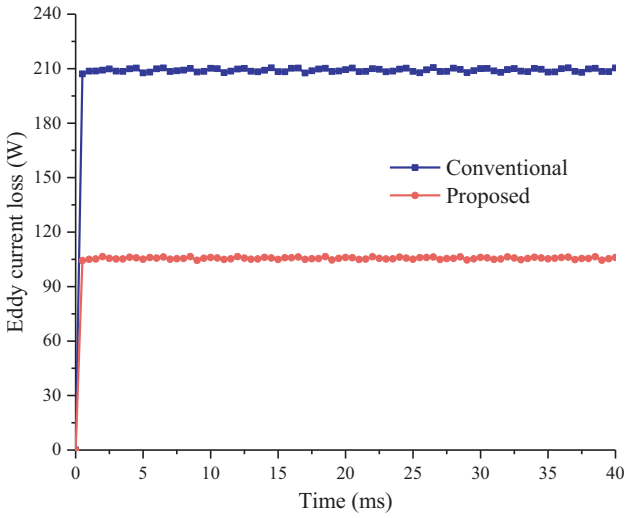

Figure 15. Eddy current loss.

and 33.14 W, respectively, and the core loss of the proposed model is 24.7% lower than that of the conventional model. In addition, from the eddy current loss diagram in Figure 15, the eddy current loss of the proposed model is 106.12 W, which is 103.46 W lower than that of the conventional model.

5. CONCLUSION

In this paper, a diesel-electric hybrid field modulation motor with bread-loaf eccentric magnetic poles for ship propulsion has been presented, and the diesel-electric hybrid ship propulsion system is analyzed. The motor model is established by the finite element method. Some key parameters of the motor are optimized by agenetic algorithm, and the electromagnetic properties such as back-EMF, torque, and loss are calculated. The contributions of this study are summarized as follows.

(1) Compared with the conventional motor, the motor has good sinusoidal back EMF; harmonic distortion of back-EMF is reduced by 3.58%; and the output torque is increased by 68.8%.

(2) Compared with the conventional motor, the inner rotor permanent magnet of the motor model adopts a bread shaped eccentric pole structure, which is embedded and fixed on the inner rotor yoke. The structure can obtain a sinusoidal air gap magnetic field. The torque ripple of the outer rotor is reduced by 1.48%, and the torque ripple of the inner rotor is reduced by 4.27%.

(3) The copper loss, iron loss, and eddy current loss of the proposed motor are reduced by 5.495 W, 6.57 W, and 103.46 W, respectively. Therefore, the proposed motor has low loss and can improve its efficiency.

REFERENCES

1. Ojaghlu, P. and A. Vahedi, "Specification and design of ring winding axial flux motor for rim-driven thruster of ship electric propulsion," *IEEE Trans. Veh. Technol.*, Vol. 68, No. 2, 1318–1326, Feb. 2019.
2. Nam, G., H. Sung, C. Kim, M. Park, and I. Yu, "Design and characteristic analysis of a 1MW superconducting motor for ship propulsions," *IEEE Trans. Appl. Supercond.*, Vol. 29, No. 5, 1–5, Aug. 2019.
3. Zhao, H., C. Liu, Z. Dong, R. Huang, and X. Li, "Design and optimization of a magnetic-geared direct-drive machine with V-shaped permanent magnets for ship propulsion," *IEEE Trans. Transport Electrific*, Vol. 8, No. 2, 1619–1633, Jun. 2022.
4. Qiao, M., C. Jiang, Y. Zhu, and G. Li, "Research on design method and electromagnetic vibration of six-phase fractional-slot concentrated-winding PM motor suitable for ship propulsion," *IEEE Access*, Vol. 4, 8535–8543, 2016.
5. Banaei, M., M. Rafiei, J. Boudjadar, and M. Khooban, "A comparative analysis of optimal operation scenarios in hybrid emission-free ferry ships," *IEEE Trans. Transport Electrific*, Vol. 6, No. 1, 318–333, Mar. 2020.
6. Jing, L., T. Wang, Y. Pan, C. Tan, and R. Qu, "Optimization of dual-flux-modulator magnetic gear with HTS bulks and uneven segment based on GA," *IEEE Trans. Appl. Supercond.*, Vol. 32, No. 6, 1–5, Sept. 2022.
7. Afsari Kashani, S. A., "Design and optimization of coaxial reluctance magnetic gear with different rotor topologies," *IEEE Trans. Ind. Electron.*, Vol. 69, No. 1, 101–109, Jan. 2022.
8. Jing, L., W. Tang, T. Wang, T. Ben, and R. Qu, "Performance analysis of magnetically geared permanent magnet brushless motor for hybrid electric vehicles," *IEEE Trans. Transport Electrific*, Vol. 8, No. 2, 2874–2883, Jun. 2022.
9. Wang, M., C. Tong, Z. Song, J. Liu, and P. Zheng, "Performance analysis of an axial magnetic-field-modulated brushless double-rotor Machine for hybrid electric vehicles," *IEEE Trans. Ind. Electron.*, Vol. 66, No. 1, 806–817, Jan. 2019.
10. Bai, J., P. Zheng, C. Tong, Z. Song, and Q. Zhao, "Characteristic analysis and verification of the magnetic-field-modulated brushless double-rotor machine," *IEEE Trans. Ind. Electron.*, Vol. 62, No. 7, 4023–4033, Jul. 2015.

11. Hwang, C. C., L. Y. Lyu, C. T. Liu, and P. L. Li, "Optimal design of an SPM motor using genetic algorithms and taguchi method," *IEEE Trans. Magn.*, Vol. 44, No. 11, 4325–4328, Nov. 2008.
12. Ho, S. L., N. Chen, and W. N. Fu, "An optimal design method for the minimization of cogging torques of a permanent magnet motor using FEM and genetic algorithm," *IEEE Trans. Appl. Supercond.*, Vol. 20, No. 3, 861–864, Jun. 2010.
13. Jolly, L., M. A. Jabbar, and Q. Liu, "Design optimization of permanent magnet motors using response surface methodology and genetic algorithms," *IEEE Trans. Magn.*, Vol. 41, No. 10, 3928–3930, Oct. 2005.
14. Jo, S., H. Shin, and J. Chang, "Dynamic analysis of surface-mounted permanent magnet type coaxial magnetic gear with damper bar considering magnetic field modulation effect," *IEEE Access*, Vol. 10, 33616–33627, 2022.
15. Jing, L., J. Gong, J. Chen, Z. Huang, and R. Qu, "A novel coaxial magnetic gear with unequal Halbach arrays and non-uniform air gap," *IEEE Trans. Appl. Supercond.*, Vol. 30, No. 4, 1–5, Jun. 2020.
16. Hua, Y., H. Zhu, M. Gao, and Z. Ji, "Multi-objective optimization design of permanent magnet assisted bearingless synchronous reluctance motor using NSGA-II," *IEEE Trans. Ind. Electron.*, Vol. 68, No. 11, 10477–10487, Nov. 2021.
17. Zhao, W., Z. Yang, Y. Liu, and X. Wang, "Analysis of a novel surface-mounted permanent magnet motor with hybrid magnets for low cost and low torque pulsation," *IEEE Trans. Magn.*, Vol. 57, No. 6, 1–4, Jun. 2021.
18. Zhou, X., X. Zhu, W. Wu, Z. Xiang, Y. Liu, and L. Quan, "Multi-objective optimization design of variable-saliency-ratio PM motor considering driving cycles," *IEEE Trans. Ind. Electron.*, Vol. 68, No. 8, 6516–6526, Aug. 2021.